ADVANCED OXIDATION PROCESSES FOR WATER/WASTEWATER TREATMENT

CrossMark

Enhanced photocatalytic activity using GO/TiO$_2$ catalyst for the removal of DCA solutions

Paula Ribao [1] · Maria J. Rivero [1] · Inmaculada Ortiz [1]

Abstract

This work aimed to optimize high-performance photocatalysts based on graphene oxide/titanium dioxide (GO/TiO$_2$) nanocomposites for the effective degradation of aqueous pollutants. The catalytic activity was tested against the degradation of dichloroacetic acid (DCA), a by-product of disinfection processes that is present in many industrial wastewaters and effluents. GO/TiO$_2$ photocatalysts were prepared using three different methods, hydrothermal, solvothermal, and mechanical, and varying the GO/TiO$_2$ ratio in the range of 1 to 10%. Several techniques were applied to characterize the catalysts, and better coupling of GO and TiO$_2$ was observed in the thermally synthesized composites. Although the results obtained for DCA degradation showed a coupled influence of the composite preparation method and its composition, promising results were obtained with the photocatalysts compared to the limited activity of conventional TiO$_2$. In the best case, corresponding to the composite synthesized via hydrothermal method with 5% of GO/TiO$_2$ weight ratio, an enhancement of 2.5 times of the photocatalytic degradation yield of DCA was obtained compared to bare TiO$_2$, thus opening more efficient ways to promote the application of photocatalytic remediation technologies.

Keywords Dichloroacetic acid · Graphene oxide · Titanium dioxide · Photocatalytic activity · Pollutants removal · Advanced oxidation process

Introduction

Water pollution is a global issue for researchers and the global environmental safety community. A grand challenge in sustaining modern society is to secure adequate water resources of desirable quality for various designated uses. The social, economic, and environmental impacts of past water resource development and inevitable prospects of water scarcity are driving the shift to a new paradigm in water resource management. New approaches incorporating the principles of sustainability have motivated the search for technological solutions to provide society with ample water sources while protecting existing resources. In this context, new technologies to alleviate water shortages and provide quality water as well as new designs and re-engineering of existing water facilities play major roles (Ortiz et al. 2015). Dichloroacetic acid (DCA) is a persistent pollutant found in water as a disinfection by-product; it is present in many industrial wastewaters and effluents and has been identified as an intermediate product in the biological degradation pathway of many chlorinated hydrocarbons, such as trichloroacetic acid, perchloroethylene, and trichloroethylene. Therefore, DCA is a prominent haloacetic acid and, according to animal studies, a more potent carcinogen than trihalomethanes (Marugán et al. 2007; Zalazar et al. 2007).

Over the past decades, a group of new technologies called advanced oxidation processes (AOPs) has been widely reported because of their high effectiveness in the oxidation of organic compounds (Bhatia and Dhir 2016; Carbajo et al. 2014). AOPs are based on the in situ generation of strongly reactive and oxidizing free radicals (Comninellis et al. 2008; Fernández-Castro et al. 2015). Among these technologies, heterogeneous

✉ Inmaculada Ortiz
  inmaculada.ortiz@unican.es

1 Department of Chemical and Biomolecular Engineering, ETSIIT, University of Cantabria, Santander, Spain

photocatalysis has attracted increasing attention worldwide for wastewater environmental problems, air purification, CO_2 reduction, and water splitting because it can be driven by solar energy (Wen et al. 2015; Moreira et al. 2012). Among various semiconductors used, commercial TiO_2 presents several advantages in environmental applications (Pelaez et al. 2012; Lee and Park 2013) because it is highly photoreactive and cost-effective. Moreover, it presents high chemical stability in a wide pH range, strong resistance to chemical breakdown and photo corrosion, and commercial availability (Chatterjee and Dasgupta 2005; Chong et al. 2010; Kumar and Devi 2011; Nakata and Fujishima 2012; Chen et al. 2012; Byrne et al. 2017). The increasing demand for clean photocatalysis to mitigate environmental problems, particularly by organic contaminants, has created high demand for TiO_2-based photocatalysts. However, the photocatalytic activity of this solid remains limited by some disadvantages. Due to the relatively wide band gap energy of 3.2 eV, TiO_2 only absorbs radiation in the ultraviolet region (Rodríguez-Chueca et al. 2015), which represents 4 to 8% of the solar spectrum (Mendiola-Alvarez et al. 2017; Janani et al. 2016; Adán et al. 2015). In addition, a large fraction (90%) of electron-hole pairs recombine within a nanosecond of their generation, and only a few are able to migrate to the semiconductor surface for the production of reactive species (Friedman et al. 2010).

Graphene and its derivatives, as graphene oxide (GO), have recently emerged as one of the most promising candidates for the development of photo-efficient composite catalysts (Cruz et al. 2017). Graphene oxide, a perfectly functionalized graphene produced by chemical exfoliation, is a single-atom-thick sheet arranged by localized sp^3 defects within the sp^2-bonded carbon atoms in a hexagonal lattice with two-dimensional planar sheets (Jiang et al. 2013). Functional graphene can be prepared through solution-based processes at low cost, which provides significant opportunities for functionalized graphene-based composite materials (Morales-Torres et al. 2012). Graphene oxide can easily react with TiO_2 and be reduced to conductive graphene. The coupling of these materials presents four advantages in terms of photocatalytic activity: (i) graphene oxide can trap and move charge carriers, thus avoiding recombination of the electron-hole pairs; (ii) the composite can be easily recovered from aqueous solution due to the large GO sheets; (iii) band gap tuning and/or extension of the excitation wavelength can be achieved; and (iv) the new composite provides an adequate quality and quantity of active sites. Elemental carbon is transferred into the lattice of TiO_2 by replacing some Ti atoms and forms C–O or C=O bonds in the process of doping, which produces a hybrid orbital just below the conduction band of TiO_2 and enhances the utilization efficiency of visible light (Leary and Westwood 2011; Liu et al. 2013).

Some papers focused on the enhancement of the photocatalytic activity using GO/TiO_2 composites can be found in the literature. However, no clear conclusions have been obtained so far due to the different experimental methods and GO/TiO_2 weight ratio, which could influence the properties of the catalyst. Szabó and co-workers (2013) and Wojtoniszak and co-workers (2012) reported better photocatalytic activity of the TiO_2 than the composite. On the other hand, Li and co-workers (2013) and Liang and co-workers (2014) found photocatalytic improvement using the composite. Morales-Torres and co-workers (2013) synthesized GO/TiO_2 composites with different amounts of GO in relation to TiO_2 ranging from 1 to 6%, finding the best photocatalytic degradation of methyl orange with a GO/TiO_2 weight ratio of 1.4%. However, composites with a GO/TiO_2 weight ratio of 5% provided the best photoactivity under visible light in the degradation of methylene blue according to the work developed by Liu and co-workers (2013). Therefore, the scattering and the somehow contradictory results previously reported make it necessary to deeply analyze the potential enhancement of the composites photocatalytic activity.

This work focuses on the synthesis and optimization of new photocatalysts based on GO/TiO_2 composites that show enhanced performance in the degradation of DCA, a persistent aqueous pollutant, in comparison with the most widely used form of TiO_2.

Materials and methods

Materials

Graphite powder was purchased from ACROS ORGANICS. Sulfuric acid 95–98% (H_2SO_4), hydrochloric acid 37% (HCl), potassium permanganate ($KMnO_4$), and sodium nitrate ($NaNO_3$) were provided by Panreac. Hydrogen peroxide (H_2O_2, 30% *v/v*) was purchased from Scharlau. DCA was provided by Sigma-Aldrich, and titanium dioxide (P25, 20% rutile and 80% anatase) was purchased from Evonik Degussa.

Synthesis of graphene oxide

To prepare GO, natural graphite was oxidized according to modified Hummers' method (Hummer and Hoffeman 1958). Graphite (3 g) and sodium nitrate (1.5 g) were added to concentrated sulfuric acid (70 mL) under stirring at 0 °C inside a cooling bath. Potassium permanganate (9 g) was added slowly to maintain a suspension temperature of less than 20 °C under vigorous stirring. Next, the reaction was heated to 35 °C for 30 min. Then, 50 mL of deionized water was added, and the temperature was increased to 98 °C. This temperature was maintained for 15 min under stirring. Another 170 mL of deionized water was added, followed by 4 mL of H_2O_2 (30%). A purification step was then performed in which the mixture was centrifuged and washed with 200 mL of deionized water and HCl aqueous solution (10% *v/v*, 80 mL) to

remove metal ions. The remaining solid was sonicated to obtain exfoliated graphene oxide nanosheets, the sample was centrifuged again, and the supernatant was collected and dried in an oven (50 °C) overnight.

Synthesis of GO/TiO$_2$ composites

Three types of composites were synthesized via different synthesis methods. In the mechanical method (M), GO/TiO$_2$ composites were prepared by mixing and sonication. Briefly, P25 was added to a GO aqueous dispersion under vigorous stirring for 1 h. The obtained suspension was sonicated for 1 h, yielding a homogeneous gray suspension. The sample was then washed and dried overnight at 50 °C.

The GO/TiO$_2$ composite was also obtained via a hydrothermal method (H). In brief, 0.6 g of TiO$_2$ was added to the GO dispersion (6, 30, and 60 mg of GO for 1, 5, and 10% of GO/TiO$_2$ weight ratio, respectively). After stirring for 2 h, the solution was transferred to a 200-mLTeflon-lined stainless steel autoclave and maintained at 120 °C for 3 h. The resulting composite was recovered by centrifugation, rinsed with deionized water (DI) three times, and fully dried at 50 °C overnight.

Finally, GO/TiO$_2$ composites were also prepared via a solvothermal method (S). In a typical synthesis, GO and P25 were mixed in ethylene glycol (100 mL) and stirred for 2 h. After this time, the reaction solution was transferred to the 200-mL Teflon-lined stainless steel autoclave and incubated in an oven at 120 °C for 3 h. The composite was recovered by centrifugation and washed three times with DI water. Finally, the composite was left to dry overnight at 50 °C.

During the process, particularly during the hydrothermal and solvothermal synthesis, GO can be reduced to rGO. However, the nanocomposites are denoted hereafter as H, S, or M, referring to the hydrothermal, solvothermal, or mechanical preparation method, respectively; 1, 5, or 10% indicates the GO/TiO$_2$ weight ratio used in the preparation.

Composite characterization

Atomic force microscopy (AFM) images were obtained with a Park Systems XE-100 microscope in true non-contact mode with a plastic substrate. Transmission electron microscopy (TEM) observations were performed on a JEOL JEM-2100 electron microscope. Fourier transform infrared (FTIR) spectra were recorded on a Spectrum Two spectrometer (Perkin Elmer). Raman spectra were recorded by a T64000 Triple Raman Spectrometer (HORIBA) with a 514-nm laser. X-ray diffraction (XRD) was performed on a Bruker D8 Advance diffractometer equipped with Cu Kα radiation ($\lambda = 1.5418$ Å) to determine the crystal structures of the prepared composites. Thermogravimetric analysis (TGA) of GO/TiO$_2$ composites was performed in a Shimadzu DTG-60H Differential Thermal Gravimetric Analyzer by heating the sample in

nitrogen flow from 25 to 910 °C at 20 °C min^{-1}. The band gap of the samples was calculated by UV/vis diffuse reflectance spectroscopy using a Cary 5000 UV-vis-NIR spectrophotometer (Agilent Technologies) equipped with a sphere diffuse reflectance accessory model 5000. The specific surface area of the solids was measured by the Brunauer-Emmett-Teller (BET) method from nitrogen adsorption-desorption data with an adsorption apparatus (Micromeritics, ASAP 2000).

Photocatalytic activity

Photocatalytic experiments were conducted in a 1-L Heraeus Laboratory UV Reactor mounted on an Agimatic-S magnetic stirring plate (JP Selecta, Spain). The light source, which was immersed in a quartz sleeve placed in the center of the reactor, was a 150-W medium-pressure Hg lamp (Heraeus Noblelight TQ 150 z1) with an emission spectrum between 200 and 600 nm and a maximum emission at 366 nm. The irradiation on the reactor wall was measured with a radiometer PHD2102.11 (Delta OHM), obtaining values of 97.30, 35, 1, and 452.4 Wm^{-2} for UV-A, UV-B, UV-C, and visible light, respectively.

Preliminary adsorption experiments were performed by mixing 0.8 L of 1000 mgL^{-1} DCA solution and the catalyst under no radiation for 24 h; subsequently, the synthesized composites were tested by mixing 0.8 L of 1000 mgL^{-1} DCA solution with 0.3 gL^{-1} composites. The selected concentration of the catalyst was within the range of values previously analyzed by different researchers, 0.05 to 5 gL^{-1} (Krishnamoorthy et al. 2011; Liang et al. 2014; Wang et al. 2013). Once the photocatalytic degradation had begun, samples were collected at different time intervals and filtered through a 0.45-μm syringe filter (Teknokroma). The catalyst reuse study was performed in three successive photocatalytic cycles, and the catalyst was recovered via centrifugation. The DCA concentration was measured in an ICS-1100 (Dionex) ion chromatograph with an AS9-HC column using a solution of Na$_2$CO$_3$ (9 mM) as the eluent at a flow rate of 1 mLmin^{-1} and a pressure of approximately 2000 psi. Dissolved organic carbon (DOC) was analyzed using a Shimadzu TOC-V CPH analyzer (Shimadzu Corp. Japan).

Results and discussion

Composite characterization

Dilute suspensions of H10% and H5% were dropped onto freshly cleaved mica and then analyzed using AFM; the results are shown in Fig.1. The mica substrate was covered with GO sheets coupled to TiO$_2$ nanoparticles. The interaction between GO and TiO$_2$ occurs via carboxylic acid functional groups or simple physisorption (Wang et al. 2012). The height
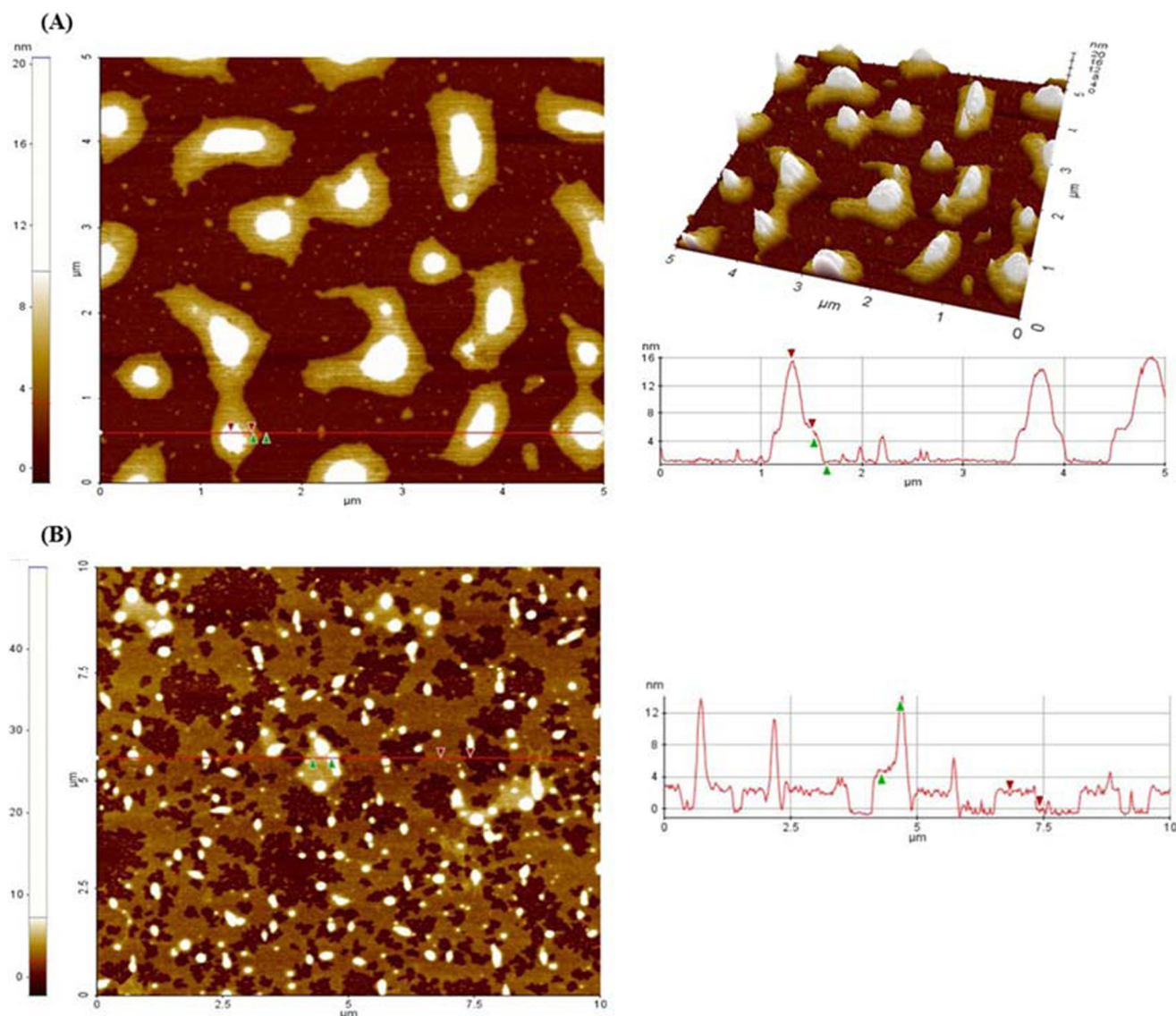
Fig. 1 AFM image of H10% (**a**) and H5% (**b**) composites and depth profile of the line of interest on the GO/TiO$_2$ solid

profiles showed 4-nm-thick GO nanoplatelets decorated with TiO$_2$ nanoparticles with an average diameter of 10 nm for H10% composite. Stankovich et al. (2007) reported that the thickness of a single sheet of GO is typically 0.6–1.3 nm, indicating that the GO obtained might be a trilayer sheet. However, the H5% composite showed 2-nm-thick GO nanoplatelets and TiO$_2$ nanoparticles with an average diameter of 10 nm. This fact indicates that in the case of H5%, GO is formed by the stacking of only two sheets, leading to the conclusion that a better exfoliation of GO was indeed achieved under these conditions.

GO/TiO$_2$ composites were further examined using transmission electron microscopy. Figure 2a shows the TEM images of the solid H5%; the TiO$_2$ nanoparticles were dispersed on the graphene oxide plane, which exhibited a flake-like

structure with some wrinkles. Figure 2b–d presents EDX spectra collected from areas S1, S2, and S4 in Fig. 2a. The composition of the graphene oxide sheets (S1) was carbon with a minor proportion of oxygen. The S2 area exhibited a composition of titanium and oxygen, demonstrating the presence of TiO$_2$ on the graphene oxide nanosheets. Finally, no elements were detected in area S4, demonstrating that the titanium dioxide was only found coupled to graphene oxide nanosheets. The copper signal is attributable to the sample support.

Figure 3a shows the FTIR spectra of the samples TiO$_2$, GO, H5%, S5%, and M5%. The GO spectrum showed many strong absorption peaks corresponding to various oxygen functional groups. The peaks at 3400 and 1620 cm^{-1} were ascribed to the stretching vibration of water hydroxyl groups
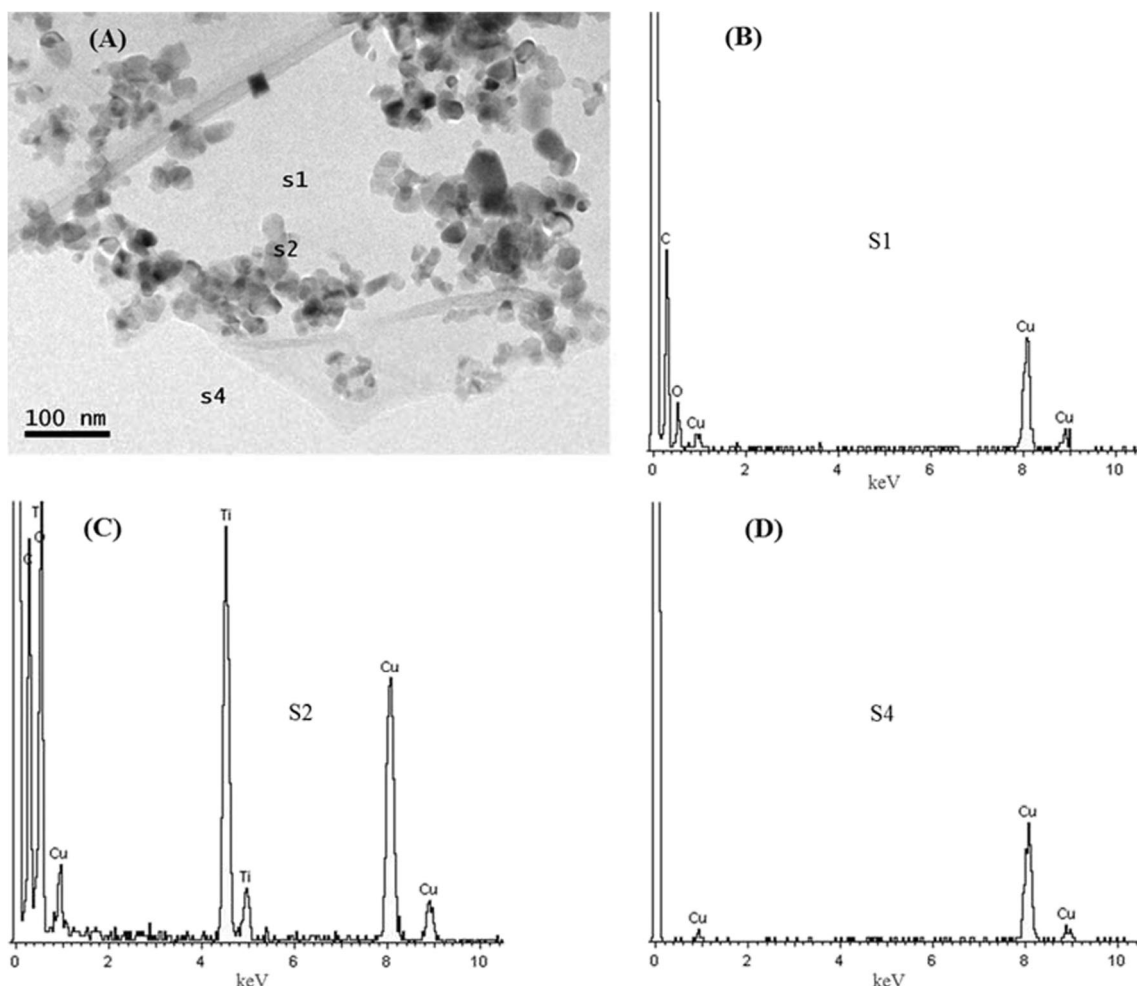
Fig. 2 TEM image of the composite H5% (a) and EDX scanning corresponding to zones S1 (b), S2 (c), and S4 (d) in the image

and the skeletal vibration of C=C, respectively. The other peaks at 1732, 1380, 1220, and 1055 cm^{-1} were assigned to carboxylate C=O stretching, carboxyl C–O, epoxide C–O–C or henolic C–O–H, and alkoxy C–O, respectively (Liang et al. 2014; Zhang et al. 2012). In the H5% and S5% spectra, the intensity of all absorption peaks corresponding to oxygen functional groups presented a significant decrease compared with the spectrum of bare graphene oxide, implying that GO was significantly reduced to rGO during thermal treatment. For M5%, the spectrum showed that the composite retained peaks corresponding to oxygen groups, indicating that GO had not been reduced to rGO. Therefore, the ability of the solid M5% to transport electrons is expected to be lower than those of H5% and S5%. In addition, all composites presented high peaks at 500–900 cm^{-1} that were attributed to the stretching vibrations of Ti–O–Ti and Ti–O–C bonds. Therefore, the above results confirmed the successful preparation of GO/TiO$_2$ composites via hydrothermal and solvothermal treatments; however, the composites synthesized using the mechanical method are not expected to exhibit high photocatalytic activity because reduction of GO was not observed.

The presence of graphene oxide and TiO$_2$ in the composites was further confirmed by Raman spectroscopy (Fig. 3b). The spectra of the composites presented four peaks in the region below 800 cm^{-1}, with three modes of vibration matching to symmetry B$_{1G}$, A$_{1g}$, and E$_g$, corresponding to the crystalline phase anatase. In addition, two extra peaks were observed at 1353 cm^{-1} (D peak) and 1576 cm^{-1} (G peak), confirming the presence of graphene oxide in the samples. The composites presented an increased area under the D curve relative to the GO sample (Table A1—Online Resource), suggesting the formation of more sp^3 defects in carbon. The defects in the GO sheets were clearly not well repaired during the synthesis step and remained after the removal of oxygen groups. The increased sp^3 defects might be attributable to the strong interaction (Ti–O–C bonds) at the interface of the TiO$_2$ nanoparticles and GO sheets (Wang et al. 2013). Furthermore, the catalyst M5% presented the highest area under D curve and hence exhibited the highest concentration of sp^3 aggregates. This may be due to the incomplete reduction of GO during the preparation step, which led to the persistence of some oxygen groups on the GO surface. In the Raman spectrum of H5%, a systematic variation of the frequency of D and G to lower
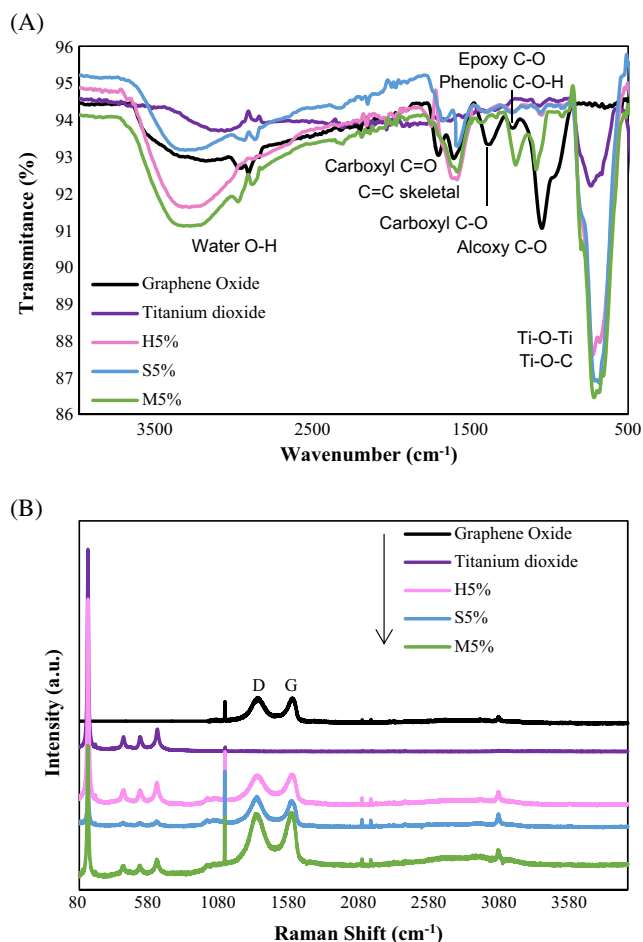
Fig. 3 FTIR spectra (a) and Raman spectroscopy (b) of graphene oxide, titanium dioxide, H5%, S5%, and M5%

wavelengths and a significant increase in the full width at half maximum (FWHM) of the same bands were also observed (Table A1—Online Resource). These features are associated with charge transfer processes in GO. When the frequency moves to lower wavelength, charge transfer occurs due to electron mobility. In the case of S5%, the charge transfer process was less clear. Therefore, lower photocatalytic activity could be expected.

Thermal gravimetric analysis (TGA) of TiO$_2$, GO, H1%, H5%, and H10% in a N$_2$ atmosphere is shown in Fig. A1 (Online Resource). The thermogravimetric curve of GO presented three differentiated steps of mass loss with temperature in the range from ambient temperature to 900 °C. The first step corresponds to desorption of physically absorbed water below 100 °C. Between 200 and 250 °C, the mass loss is attributable to the removal of oxygen-containing groups. Finally, the third mass loss step observed around 500 °C is due to the destruction of the carbon skeleton (carbonyl/double bond) of graphene oxide (Li et al. 2013; Xu et al. 2014). The catalysts H1%, H5%, and H10% exhibited displacements of

the onsets of weight loss relative to GO and exhibited weight loss roughly parallel to that of GO across the temperature range examined. These results suggest that GO was initially stabilized by the embedded TiO$_2$, which delayed the weight loss normally observed in the thermal analysis of GO samples (Lambert et al. 2009). Subsequent determination of the content of graphene oxide in the photocatalysts by TG analysis revealed that 3.87, 7.27, 10.95, 5.62, and 5.59% graphene oxide was present in H1%, H5%, H10%, S5%, and M5%, respectively.

To determine the specific surface area of the composite nanomaterial, N$_2$ adsorption/desorption measurements and the Brunauer-Emmet-Teller (BET) analysis method were used. The nitrogen adsorption/desorption isotherms of the composites showed an overall shape of type H3, which corresponds to materials with mesoporous and macroporous characteristics. This type of hysteresis cycle is characteristic of materials with sheet morphology and flexible pores. All composites showed an increment in surface area values compared with TiO$_2$. The specific area increased with increasing GO/TiO$_2$ weight ratio, reaching specific areas up to 66.71, 68.24, and 62.37 m^{2}g^{-1} for H10%, S10%, and M10%, respectively (Table A2—Online Resource). These observations are in agreement with other works reporting an increment of up to 20% in the specific area values (Morales-Torres et al. 2013; Wang et al. 2012). There were no significant variations in surface area among the fabricated composites; therefore, the influence of this variable on the photocatalytic activity of the composites could not be analyzed.

XRD analyses were performed to analyze the crystal phases of the TiO$_2$ and H5% (Fig. 4). TiO$_2$ and H5% presented the same characteristic crystal planes of anatase and rutile phases. This means that TiO$_2$ structure was not modified by the addition of graphene oxide nanosheets. A diffraction peak at 2θ value around 11.3° was observed in the GO curve, indicating the possible existence of trapped water between the layers of hydrophilic GO. This peak is not observed in H5% composite because during the synthesis step, the trapped water is removed.

The band gaps of the TiO$_2$ and composites were estimated from the plots of $[F(R)h\nu]^{1/2}$ versus $h\nu$. The Kubelka Munk function $F(R)$ is proportional to the equivalent absorption coefficient and is obtained by converting the reflectance according to the following equation:

$$F(R) = \frac{(1-R)^2}{2R} \qquad (1)$$

Figure A2 (Online Resource) shows that the band gap of pure TiO$_2$ was 3.25 eV, whereas the band gaps of the composites were significantly reduced (Table A2—Online Resource). The value of the band gap decreased after anchoring TiO$_2$ onto
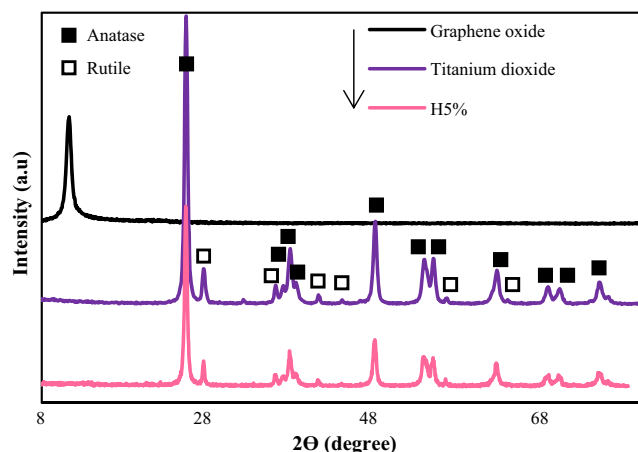
Fig. 4 XRD patterns of graphene oxide, titanium dioxide, and H5%

Fig. 5 Proposed reaction scheme of DCA oxidation

the graphene oxide sheet, resulting in composites able to absorb visible light up to 440 nm. This phenomenon is the result of the different interaction intensities of C–O and C–Ti during the synthesis process. In the thermal process, Ti and O atoms interact more actively with graphene oxide than in the mechanical procedure. The disappearance of the functional groups on the GO surface, as confirmed by FTIR analysis, prevents the π electrons of the C atom from binding other atoms to form a delocalized large π bond. Consequently, the remaining unpaired π electrons are bound with more free Ti and O atoms on the surface of TiO_2. This interaction should result in the significant reduction of the band gap of the composites (Lee et al. 2012; Ni et al. 2014). Moreover, in a previous work (Ribao et al. 2017), it was reported that bare TiO_2 nanoparticles do not present photocurrent response under visible light, while H5% catalysts showed high photocurrent values. Therefore, it is possible to expect higher activity during DCA degradation. So far, it can be considered that the improved photoresponse of the H5% composite presumably benefits the charge transport, avoiding the recombination rates of electron-hole pairs.

Thus, the results of the characterization revealed significant differences between the newly synthesized GO/TiO_2 composites that were related both to the synthesis method used and the graphene oxide content employed.

Photocatalytic activity

Mechanism of DCA photocatalytic oxidation using GO/TiO_2 composites

Figure 5 shows the proposed reaction scheme of the photocatalytic process using GO/TiO_2 as the catalyst. Under UV-vis light irradiation, the electron in the valence band is promoted to the conduction band of TiO_2, and the photogenerated electron on the conduction band
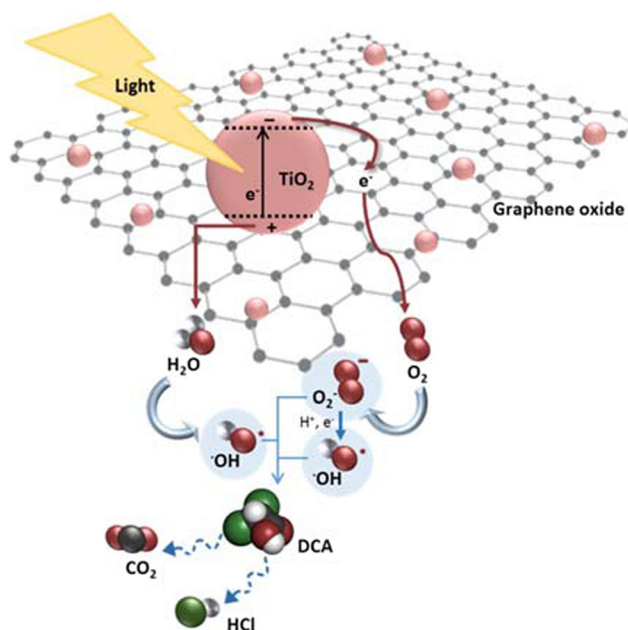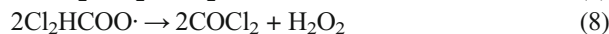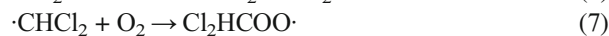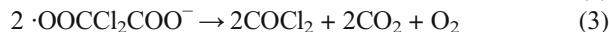
can effectively reduce oxygen via the graphene oxide nanosheets to form superoxide radicals ($O_2{}^{\cdot-}$). In this case, the GO nanosheets function as a co-catalyst for the rapid transfer of the photogenerated electrons from TiO_2, which results in a lower recombination rate and enhanced photocatalytic activity. $O_2{}^{\cdot-}$ radicals can induce the generation of hydroxyl radicals ($\cdot OH$) through an intermediate peroxide process. Second, the hole in the valence band generates hydroxyl radicals through water oxidation. Finally, the reactive species attack DCA, leading to its degradation and mineralization following the next alternatives (Zalazar et al. 2007; Lovato et al. 2011):

1. $CCl_2HCOO^- + \cdot OH \rightarrow \cdot CCl_2COO^- + H_2O$ (1)

    $\cdot CCl_2COO^- + O_2 \rightarrow \cdot OOCCl_2COO^-$ (2)
    $2 \cdot OOCCl_2COO^- \rightarrow 2COCl_2 + 2CO_2 + O_2$ (3)
    $COCl_2 + H_2O \rightarrow CO_2 + 2HCl$ (4)

2. $CCl_2HCOO^- + \cdot OH \rightarrow CCl_2HCOO\cdot + {}^-OH$ (5)

    $CCl_2HCOO\cdot \rightarrow \cdot CHCl_2 + CO_2$ (6)
    $\cdot CHCl_2 + O_2 \rightarrow Cl_2HCOO\cdot$ (7)
    $2Cl_2HCOO\cdot \rightarrow 2COCl_2 + H_2O_2$ (8)

Therefore, coupling graphene oxide and titanium dioxide should contribute to the effective separation and high-efficiency utilization of photogenerated electrons, thus improving the photocatalytic performance of the GO/TiO_2 photocatalysts.

Fig. 6 DCA degradation percentages after 8 h of irradiation time and kinetic constants values for each photocatalyst
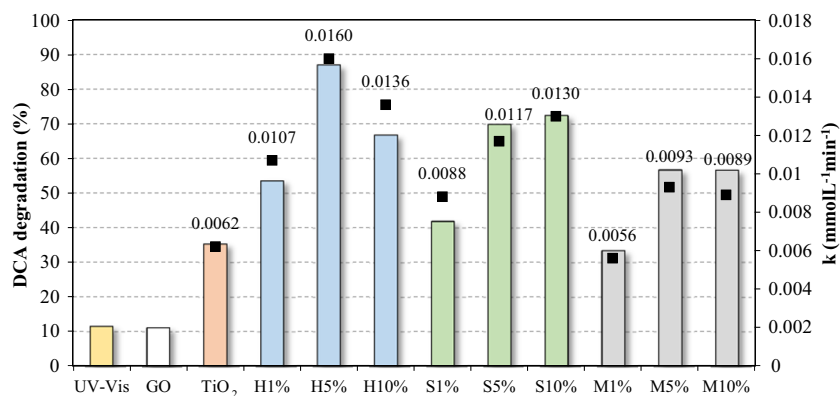
Photocatalytic degradation of DCA using the novel synthesized composites

The photocatalytic degradation of DCA with the novel composites was measured under UV-vis light. First, the experimental error was determined to be less than 2%. Preliminary experiments of dark adsorption of the target compound onto the catalyst showed that after 24 h of contact, there was no significant adsorption of DCA on titanium dioxide or on the composite (Fig. A3—Online Resource).

The experimental data of DCA degradation were fitted to a zero-order kinetic model in all cases except in the study without catalyst or when only GO was employed. Figure 6 shows the DCA degradation percentage and kinetic constants for 8 h of treatment. It can be observed that DCA cannot be degraded by pure GO. Commercial TiO$_2$ exhibited lower photocatalytic activity than the novel composites in all cases. After coupling between GO and TiO$_2$, the photocatalytic degradation in the studied time was improved from 35.37 to 87.10%; the maximum value corresponds to the photocatalyst H5%, increasing the degradation rate 2.6 times. Moreover, for a given GO/TiO$_2$ weight ratio, there was a significant influence of the synthesis method on the photocatalytic activity, especially in the case of composites with a GO/TiO$_2$ weight ratio of 5%.

The catalysts H5% and S5% improved the photocatalytic performance to maxima of 87.10 and 69.89% DCA degradation, respectively. By contrast, the catalyst M5% only achieved 56.74% of DCA degradation after 8 h of treatment.

The use of a small amount of graphene oxide was not sufficient to achieve significant improvement in the photocatalytic degradation of DCA (Wang et al. 2010), regardless of the synthesis method. The catalyst H5%, which was synthesized via the hydrothermal method with a GO/TiO$_2$ weight ratio of 5%, presented optimal photocatalytic activity and exhibited the highest performance among all prepared materials. These superior results may be due to the charge transfer process observed in the Raman spectra of the hydrothermal composites, which was not as clearly observed for the catalyst

S5%. The composite M5% exhibited worse behavior because the coupling between GO and TiO$_2$ was not adequate and the graphene oxide was not completely reduced during synthesis, as confirmed by the FTIR spectra. Further, increasing the GO/TiO$_2$ weight ratio to 10% to obtain the solids H10% and M10% led to a decrease in the degradation rate compared with the catalysts H5% and M5%, although the degradation rate remained higher than that obtained with TiO$_2$ and with the composites H1% and M1%. Therefore, a high GO load may act as a shield that increases opacity, resulting in a decrease in the irradiation that passes through the suspension. However, the solid S10% exhibited higher photocatalytic activity than the solid S5% as well as slightly higher photocatalytic activity than the catalyst H10%. This higher activity may be due to the greater dispersion of large amounts of GO in ethylene glycol than in water during the synthesis step, which provided a greater contact area between the TiO$_2$ and GO. Therefore, the results obtained for DCA photocatalytic oxidation revealed a coupled influence of the composite preparation method and GO loading, with promising results compared to the limited activity of conventional TiO$_2$. Furthermore, analysis
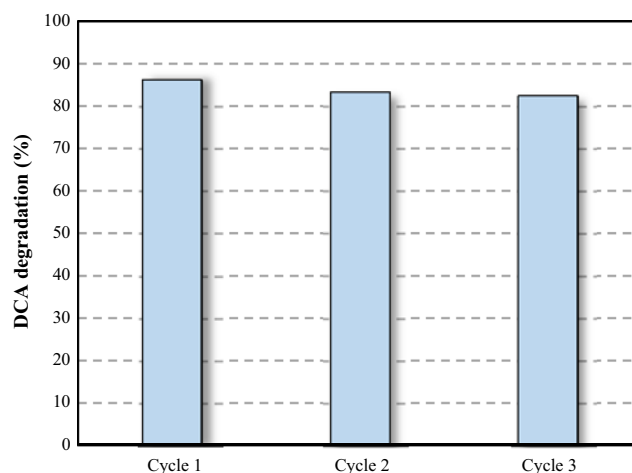

Fig. 7 DCA degradation over the catalyst H5% for three successive photocatalytic runs

of DCA mineralization based on changes in DOC revealed that the measured values matched undegraded DCA (Fig. A4—Online Resource).

To confirm the performance stability and reusability of the composites, the photocatalytic oxidation of DCA was analyzed in three different cycles using the catalyst H5%. The results are shown in Fig. 7; the catalyst maintained stable and effective photocatalytic activity, with a total photocatalytic activity loss of 4.3% after the third cycle.

Conclusions

Environmental photocatalytic applications of GO/TiO_2 nanocomposites have evoked great interest due to the improved performance of these nanocomposites compared to conventional TiO_2 particles. In this work, nine novel composites were synthesized by varying the GO/TiO_2 weight ratio in the range of 1 to 10% and following three different preparation methods, hydrothermal, solvothermal, and mechanical, to obtain an optimized GO/TiO_2 photocatalyst. Performance was assessed based on the degradation of DCA, a disinfection by-product, which revealed an improved degradation rate for the new composites compared with bare TiO_2. Catalysts with a weight ratio of 1% provided the worst photocatalytic results among the newly synthesized catalysts, probably due to an insufficient graphene oxide load. For the rest of the composites, the DCA degradation efficiency followed the trend H5% > S10% > S5% > H10% > M5% > M10%. Therefore, the composite H5% provided the best photocatalytic activity among all synthesized composites, with a degradation yield of 87.1% after 8 h of treatment and a degradation rate 2.6 times higher than bare TiO_2. High graphene content improved the photocatalytic activity of the catalyst S10% due to the best dispersion of large GO loads in ethylene glycol. The composites M5% and M10% displayed the worst behavior due to inadequate coupling between GO and TiO_2 and incomplete reduction of graphene oxide during the synthesis process, as confirmed by the FTIR spectra. Although the results for DCA degradation showed a coupled influence of the composite preparation method and composition, promising results were achieved. In summary, the novel optimized photocatalyst represents a successful alternative for DCA degradation compared to the limited activity of conventional TiO_2 due to the ability of GO sheets to avoid electron-hole recombination and efficiently use visible light. These results increase the potential application of photocatalysis for the remediation of polluted water and wastewaters.

References

Adán C, Marugán J, Obregón S, Colón G (2015) Photocatalytic activity of bismuth vanadates under UV-A and visible light irradiation: inactivation of Escherichia coli vs oxidation of methanol. Catal Today 240:93–99. https://doi.org/10.1016/j.cattod.2014.03.059

Bhatia V, Dhir A (2016) Transition metal doped TiO_2 mediated photocatalytic degradation of anti-inflammatory drug under solar irradiations. J Environ Eng 4(1):1267–1273. https://doi.org/10.1016/j.jece.2016.01.032

Byrne C, Subramanian G, Pillai SC (2017) Recent advances in photocatalysis for environmental applications. J Environ Chem Eng Article in press. https://doi.org/10.1016/j.jece.2017.07.080

Carbajo J, García-Muñoz P, Tolosana-Moranchel A, Faraldos M, Bahamonde A (2014) Effect of water composition on the photocatalytic removal of pesticides with different TiO_2 catalysts. Environ Sci Pollut Res 21(21):12233–12240. https://doi.org/10.1007/s11356-014-3111-5

Chatterjee D, Dasgupta S (2005) Visible light induced photocatalytic degradation of organic pollutants. J Photoch Photobio C 6(2–3):186–205. https://doi.org/10.1016/j.jphotochemrev.2005.09.001

Chen H, Nanayakkara CE, Grassian VH (2012) Titanium dioxide photocatalysis in atmospheric chemistry. Chem Rev 112(11):5919–5948. https://doi.org/10.1021/cr3002092

Chong MN, Jin B, Chow CWK, Saint C (2010) Recent developments in photocatalytic water treatment technology: a review. Water Res 44(10):2997–3027. https://doi.org/10.1016/j.watres.2010.02.039

Comninellis C, Kapalka A, Malato S, Parsons SA, Poulios I, Mantzavinos D (2008) Advanced oxidation processes for water treatment: advances and trends for R&D. J Chem Technol Biol 83(6):769–776. https://doi.org/10.1002/jctb.1873

Cruz M, Gomez C, Duran-Valle CJ, Pastrana-Martínez LM, Faria JL, Silva AMT, Faraldos M, Bahamonde A (2017) Bare TiO_2 and graphene oxide TiO_2 photocatalysts on the degradation of selected pesticides and influence of the water matrix. Appl Surf Sci 416:1013–1021. https://doi.org/10.1016/j.apsusc.2015.09.268

Fernández-Castro P, Vallejo M, San Román MF, Ortiz I (2015) Insight on the fundamentals of advanced oxidation processes. Role and review of the determination methods of reactive oxygen species. J Chem Technol Biot 90(5):796–820. https://doi.org/10.1002/jctb.4634

Friedman D, Mendive C, Bahneman D (2010) TiO_2 for water treatment: parameters affecting the kinetics and mechanisms of photocatalysis. Appl Catal B-Environ 99(3–4):398–406. https://doi.org/10.1016/j.apcatb.2010.05.014

Hummer WS, Hoffeman RE (1958) Preparation of graphitic oxide. J Am Chem Soc 8(6):1339. https://doi.org/10.1021/ja01539a017

Janani S, Sudha Rani KS, Ellappan P, Miranda LR (2016) Photodegradation of methylene blue using magnetically reduced graphene oxide bismuth oxybromide composite. J Environ Chem Eng 4(1):534–541. https://doi.org/10.1016/j.jece.2015.10.043

Jiang X, Nisar J, Pathak B, Zhao J, Ahija R (2013) Graphene oxide as a chemically tunable 2-D material for visible-light photocatalyst applications. J Catal 299:204–209. https://doi.org/10.1016/j.jcat.2012.12.022

Krishnamoorthy K, Mohan R, Kim SL (2011) Graphene oxide as a photocatalytic material. Appl Phys Lett 98(24):244101. https://doi.org/10.1063/1.3599453

Kumar SG, Devi LG (2011) Review on modified TiO_2 photocatalysis under UV/visible light: selected results and related mechanisms on

interfacial charge carrier transfer dynamics. J Phys Chem A 115(46): 13211–13241. https://doi.org/10.1021/jp204364a

Lambert TN, Chavez CA, Hernandez-Sanchez B, Lu P, Bell NS, Ambrosino A, Friedman T, Boyle TJ, Wheeler DR, Huber DL (2009) Synthesis and characterization of titania-graphene nanocomposites. J Phys Chem 113(46):19812–19823. https://doi.org/10.1021/jp905456f

Leary R, Westwood A (2011) Carbonaceous nanomaterials for the enhancement of TiO2 photocatalysis. Carbon 49(3):741–772. https://doi.org/10.1016/j.carbon.2010.10.010

Lee JK, You KH, Park CB (2012) Highly photoactive, low bandgap TiO2 nanoparticles wrapped by graphene. Adv Mater 24(8):1084–1088. https://doi.org/10.1002/adma.201104110

Lee SY, Park SJ (2013) TiO2 photocatalyst for water treatment applications. J Ind Eng Chem 19(6):1761–1769. https://doi.org/10.1016/j.jiec.2013.07.012

Li J, Zhou SL, Hong G-B, Chang C-T (2013) Hydrothermal preparation of P25-graphene composite with enhanced adsorption and photocatalytic degradation of dyes. Chem Eng J 219:486–491. https://doi.org/10.1016/j.cej.2013.01.031

Liu L, Bai H, Liu J, Sun DD (2013) Multifunctional graphene oxide-TiO2-Ag nanocomposites for high performance water disinfection and decontamination under solar irradiation. J Hazard Mater 261: 214–223. https://doi.org/10.1016/j.jhazmat.2013.07.034

Liang D, Cui C, Hu H, Wang Y, Xu S, Ying B, Li P, Lu B, Shen H (2014) One-step hydrothermal synthesis of anatase TiO2/reduced graphene oxide nanocomposites with enhanced photocatalytic activity. J Alloys Compd 582:236–240. https://doi.org/10.1016/j.jallcom.2013.08.062

Lovato ME, Martín CA, Cassano AE (2011) A reaction–reactor model for O3 and UVC radiation degradation of dichloroacetic acid: the kinetics of three parallel reactions. Chem Eng J 171(2):474–489. https://doi.org/10.1016/j.cej.2011.04.008

Marugán J, Aguado J, Gernjak W, Malato S (2007) Solar photocatalytic degradation of dichloroacetic acid with silica-supported titania at pilot-plant scale. Catal Today 129(1–2):56–68. https://doi.org/10.1016/j.cattod.2007.06.054

Mendiola-Alvarez SY, Guzmán-Mar JL, Turnes-Palomino G, Maya-Alejandro F, Hernández-Ramírez A, Hinojosa-Reyes L (2017) UV and visible activation of Cr(III)-doped TiO2 catalyst prepared by a microwave-assisted sol-gel method during MCPA degradation. Environ Sci Pollut Res 24(14):12673–12682. https://doi.org/10.1007/s11356-016-8034-x

Morales-Torres S, Pastrana-Martínez LM, Figueiredo JL, Faria JL (2013) Graphene oxide-P25 photocatalysts for degradation of diphenhydramine pharmaceutical and methyl orange dye. Appl Surf Sci 275: 361–368. https://doi.org/10.1016/j.apsusc.2012.11.157

Morales-Torres S, Pastrana-Martínez LM, Figueiredo JL, Faria JL, Silva AMT (2012) Design of graphene-based TiO2 photocatalysts—a review. Environ Sci Pollut Res 19(9):3676–3687. https://doi.org/10.1007/s11356-012-0939-4

Moreira J, Serrano B, Ortiz A, de Lasa H (2012) A unified kinetic model for phenol photocatalytic degradation over TiO2 photocatalysts. Chem Eng Sci 78:186–203. https://doi.org/10.1016/j.ces.2012.04.033

Nakata K, Fujishima A (2012) TiO2 photocatalysis: design and applications. J Photoch Photobio C 13(3):169–189. https://doi.org/10.1016/j.jphotochemrev.2012.06.001

Ni Y, Wang W, Huang W, Lu C, Xu Z (2014) Graphene strongly wrapped TiO2 for high-reactive photocatalyst: a new sight for significant application of graphene. J Colloid Interface Sci 428:162–169. https://doi.org/10.1016/j.jcis.2014.04.022

Ortiz I, Mosquera A, Lema J, Esplugas S (2015) Advanced technologies for water treatment and reuse. AICHE J 61(10):3146–3158. https://doi.org/10.1002/aic.15013

Pelaez M, Nolan NT, Pillai SC, Seery MK, Falaras P, Kontos AG, Dunlope PSM, Hamilton JWJ, Byrne JA, O'Shea K, Entezari MH, Dionysiou DD (2012) A review on the visible light active titanium dioxide photocatalysts for environmental applications. Appl Catal B-Environ 125:331–349. https://doi.org/10.1016/j.apcatb.2012.05.036

Ribao P, Rivero MJ, Ortiz I (2017) TiO2 structures doped with noble metals and/or graphene oxide to improve the photocatalytic degradation of dichloroacetic acid. Environ Sci Pollut Res 24(14):12628–12637. https://doi.org/10.1007/s11356-016-7714-x

Rodríguez-Chueca J, Ferreira LC, Fernandes JR, Tavares PB, Lucas MS, Peres JA (2015) Photocatalytic discolouration of Reactive Black 5 by UV-A LEDs and solar radiation. J Environ Chem Eng 3(4):2948–2956. https://doi.org/10.1016/j.jece.2015.10.019

Stankovich A, Dikin AA, Piner RD, Kohlhaas KA, Kleinhammes A, Jia Y, Wu Y, Nguyen ST, Ruoff RS (2007) Synthesis of graphene-based nanosheets via chemical reduction of exfoliated graphite oxide. Carbon 45(7):1558–1565. https://doi.org/10.1016/j.carbon.2007.02.034

Szabó T, Veres A, Cho E, Khim J, Varga N, Dekany I (2013) Photocatalyst separation from aqueous dispersion using graphene oxide/TiO2 nanocomposites. Colloid Surface A 433:230–239. https://doi.org/10.1016/j.colsurfa.2013.04.063

Wang D, Li X, Chen J, Tao X (2012) Enhanced photoelectrocatalytic activity of reduced graphene oxide/TiO2 composite films for dye degradation. Chem Eng J 198-199:547–554. https://doi.org/10.1016/j.cej.2012.04.062

Wang P, Wang J, Wang X, Yu H, Yu J, Lei M, Wang Y (2013) One-step synthesis of easy-recycling TiO2-rGO nanocomposite photocatalysts with enhanced photocatalytic activity. App Catal B-Environ 132-133:452–459. https://doi.org/10.1016/j.apcatb.2012.12.009

Wang Y, Shi R, Lin J, Zhu Y (2010) Significant photocatalytic enhancement in methylene blue degradation of TiO2 photocatalysts via graphene-like carbon in situ hybridization. App Catal B-Environ 100(1–2):179–183. https://doi.org/10.1016/j.apcatb.2010.07.028

Wen J, Li X, Liu W, Fang Y, Xie J, Xu Y (2015) Photocatalysis fundamentals and surface modification of TiO2 nanomaterials. Chin J Catal 36(12):2049–2070. https://doi.org/10.1016/S1872-2067(15)60999-8

Wojtoniszak M, Zielinska B, Chen X, Kalenczuk RJ, Borowiak-Palen E (2012) Synthesis and photocatalytic performance of TiO2 nanospheres-graphene nanocomposite under visible and UV light irradiation. J Mater Sci 47(7):3185–3190. https://doi.org/10.1007/s10853-011-6153-9

Xu X, Xu Y, Zhu J (2014) Photocatalytic antifouling graphene oxide-mediated hierarchical filtration membranes with potential applications on water purification. ACS Appl Mater Interfaces 6(18): 16117–16123. https://doi.org/10.1021/am5040945

Zalazar CS, Lovato ME, Labas MD, Brandi RJ, Cassano AE (2007) Intrinsic kinetics of the oxidative reaction of dichloroacetic acid employing hydrogen peroxide and ultraviolet radiation. Chem Eng Sci 62(21):5840–5853. https://doi.org/10.1016/j.ces.2007.06.023

Zhang Z, Yang W, Zou Z, Xu F, Wang X, Zhang B, Tang J (2012) One-pot, solvothermal synthesis of TiO2-graphene composite nanosheets. J Colloid Interface Sci 386(1):198–204. https://doi.org/10.1016/j.jcis.2012.07.068